Equivalent Circuit for Mechanical-Motion-Rectifier-Based Power Take-off in Wave Energy Harvesting

Chien-An Chen[#1], Xiaofan Li[*], Lei Zuo[*], Khai Ngo[#]

[#]*Department of Electrical and Computer Engineering, Virginia Polytechnic Institute and State University, Blacksburg, VA, United States*

[*]*Department of Mechanical Engineering, Virginia Polytechnic Institute and State University, Blacksburg, VA, United States*

[1]cacee14@vt.edu

Abstract— **While a new type of power take-off (PTO) based on mechanical-motion-rectifier has been developed, its dynamic model is over simplified and cannot properly predict its nonlinear system characteristics. There is a need to develop a high fidelity PTO model to predict the system dynamics. An equivalent circuit would be a convenient tool to model the system behaviour and can easily apply to a circuit-based wave-to-wire (W2W) model. In this paper, a methodology for deriving a circuit-based high-fidelity model through the PTO design is introduced following by the extraction of the parameters through experimental results. Finally, the PTO circuit model is validated by the bench test results under the time domain**

Keywords— **Power take-off (PTO), wave energy converter (WEC), mechanical-electrical analogies, mechanical-motion-rectifier (MMR), wave-to-wire (W2W) models.**

I. Introduction

An electric analogue has been adopted to depict the physical dynamic to a circuit model. Especially in electric-based inter-discipline research fields such as mechatronic or energy harvesting, equivalent circuits for various applications has been developed and applied for system design [1]–[3]. An equivalent circuit model of wave energy converter (WEC) usually includes analogues of a wave to body behavior, and power take-off (PTO). The former analogue is derived from the hydrodynamic of the wave-body interaction [4] and the later from mechanical dynamic of PTO.

A new direct-drive PTO has been designed and manufactured by Virginia Tech [5] which includes a mechanical motion rectifier (MMR) gearbox that could convert the bi-directional motion from wave into an uni-directional rotation on the generator. This could increase the PTO efficiency by keeping the generator speed under high efficient operating speed. To characterize the PTO dynamics with the non-linear MMR gearbox, simple circuit model has been developed under shock absorber applications [6]. While the model is over simplified, it is unable to accurately predict the system dynamic especially the PTO efficiency and the peak – average force from PTO which could significantly impact the levelized cost of energy (LCOE) of the WEC system. It is necessary to develop a PTO model with a high fidelity to accurately predict the system dynamics.

This paper provides a methodology to build a high fidelity equivalent circuit for the MMR-based PTO, and also simplies the nonlinear model with an equivalent circuit model. The parameters in the circuit model are extracted through multiple testing conditions, and the resulting model with extracted parameters is validated under time domain with multiple test conditions.

II. Model of Mechanical Motion Rectifier Based Power Take-off

The design and nonlinear dynamic equations of a direct-drive PTO with MMR gearbox for a point absorber type WEC system will be introduced in this section.

A. Mechanical Structure

As illustrated in Fig. 1, the direct-drive WEC system includes two parts, the floating buoy that capture the ocean wave excitation force, and the direct-drive PTO that convert the kinetic energy into electrical energy, which is implemented inside a sealed column. If the column is assumed to be fixed corresponding to the incident wave, the relative motion will be produced between the PTO and the buoy. The relative linear motion on the push tube will drive the ball-screw, and the ball-screw nut embedded with the end of the push tube will transfer the linear reciprocal motion to a bi-directional rotational motion on the input shaft of the PTO. The MMR gearbox converts the bidirectional rotational motion on the input shaft to a uni-directional motion on the output shaft and the generator.

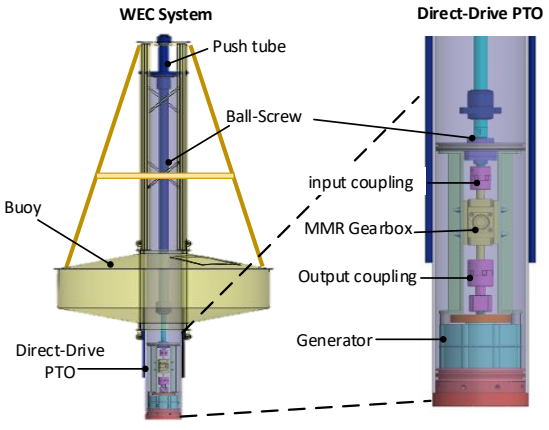

Fig. 1. Design of the single body WEC and direct-drive PTO which including the ball-screw, MMR gearbox, mechanical couplings, shafts, bearings, and permanent magnetic synchronous generator [5].

Fig. 2 shows the design of the MMR gearbox which contains two one-way sprag clutches, three bevel gears, one input shaft and one output shaft. The MMR gearbox is modified by a three-way right angle bevel gearbox to provide a high efficiency transmission [7]. The uni-directional motion transmission is the results of two one-way sprag clutches which are design to only engage in only one direction as shown in Fig. 2. The input shaft is connected to two one-way clutch on their inner rings. The inner ring (input shaft) and the outer ring (output shaft or bevel gear) of the clutch will be synchronous only when they are wedged by the sprags' friction, which is also called engagement mode. In this mode the torque will be transferred from the input shaft to the output shaft. For another direction on the inner ring, the rollers slip due to the asymmetric shape of the sprags. There is no torque transmission during this mode which is called disengagement or free-wheeling mode.

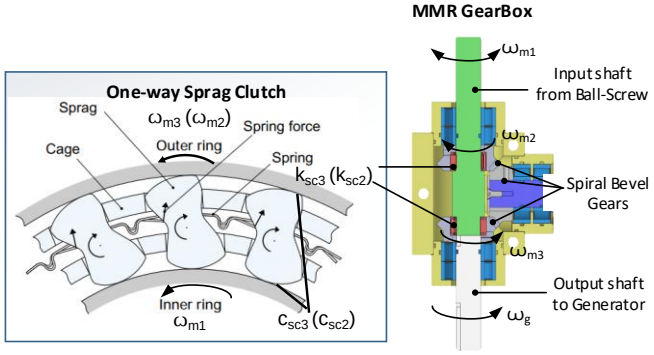

Fig. 2. The design of one-way sprag clutches in MMR gearbox where the rotational speed of the outer rings of the one-way clutches are ω_{m3} or ω_{m2}, and the rotational speed of the inner rings are ω_{m1}. The spring and the damping of the clutches are k_{sc3} (k_{sc2}) and c_{sc3} (c_{sc2}) respectively [8].

The output shaft rotates in counter-clockwise direction driven by two different ways. One way is that when the input shaft is rotating in clockwise direction, the upper clutch will engage and the lower clutch will disengage. The torque is transferred from bevel gears to the output shaft, where the bevel gears will change the rotational direction so the output shaft has opposite direction from the input shaft. Another way is that when the input shaft rotates in counter-clockwise, the upper clutch will disengage and the lower clutch will engage. The torque is directly transfer from input shaft to output shaft through the engagement of the lower one-way clutch, where the output shaft has the same rotational direction with the input shaft.

B. Mathematical Behavioral Model

To model the WEC system dynamic, a time-domain Cummins' equation (1) is used [9] for the heave-only, SDoF WEC system. As in [10], the mooring force $f_m(t)$, and non-linear viscous damping force $f_v(t)$ are usually omitted during controller design.

$$(m_f + A_{11\infty} + m_{pto})\ddot{x}_e + \int_{-\infty}^{t} k_r(t-\tau)x(\tau)d\tau + f_{pto} + k_s x_e = f_e \quad (1)$$

where $A_{11\infty}$ is the added mass in infinite frequency, shown as:

$$A_{11\infty} = \lim_{\omega\to\infty} A(\omega) \quad (2)$$

where ω is the frequency of regular wave; m is the mass of buoy; x_e is the vertical displacement of the buoy (upward as positive); $k_r(t)$ is the impulse response function of a radiation force; k_s is the hydrodynamic stiffness which results in hydrostatic force, f_{pto} is the force applied by PTO; f_e is the heave excitation wave force exerted by incident wave while the buoy is fixed.

The PTO force f_{pto} is derived from the following (3) – (10) of PTO and generator dynamics. First, the ball-screw transfer the linear speed $\dot{x_e}$ into rational speed ω_{m1}, and the gear ratio of the ball-screw k_b can be derived from the $l/2\pi$ where l is the ball-screw lead.

$$\dot{x}_e = 2\pi\omega_{m1}/l = \omega_{m1}/k_b \quad (3)$$

The f_{pto} in (4) is contributed from the Coulomb friction torque τ_0, the viscous friction c_n and c_{vs} on both ball-screw nuts and input shaft coupling, the equivalent force from the torque T_s that is transferred to the one-way clutch, the forces from Newton's second law where the mass m_{pt} and m_{bn} are from the push rod and ball-screw nut, the inertia J_{s1} and J_{cp1} are from the input shaft and the upper mechanical coupling respectively. The torque on the one-way clutch T_s is based on the nonlinear equation (5) which is decided by three different modes according to the rotational speed of input shaft ω_{m1} and its relationship with the speed of the output shaft ω_g. The physical behavioral model can be also found in the Fig. 2.

$$f_{PTO} = sgn(\dot{x}_e)\tau_0 k_b + (c_n + c_{vs}{k_b}^2)\dot{x}_e + T_s k_b + \left[m_{pt} + m_{bn} + (J_{s1} + J_{cp1}){k_b}^2\right]\ddot{x}_e \quad (4)$$

$$T_s = \begin{cases} c_{c3}(\omega_{m1} - \omega_{m3}) + k_{c3}(\theta_{m1} - \theta_{m3}) & if\ \omega_{m1} > 0 \\ c_{c2}(\omega_{m2} - \omega_{m1}) + k_{c2}(\theta_{m2} - \theta_{m1}) & if\ \omega_{m1} < 0 \\ 0 & if\ |\omega_{m1}| < \omega_g \end{cases} \quad (5)$$

where k_{c3} and k_{c2} are the spring's torsion coefficient from the cage and sprags motion in the lower and the upper one-way clutch respectively, which are linearly approximated and will be extracted from the experiments; c_{c3} and c_{c2} are the torsional damping coefficient inside the lower and the upper one-way clutch; ω_{m1} and θ_{m1} are the rotational speed and the angle of the input shaft; ω_{m2} and θ_{m2} are the rotational speed and the angle of the outer ring of the upper one-way clutch; ω_{m3} and θ_{m3} are the rotational speed and the angle of the outer ring of the lower one-way clutch. The relationship of the rotational speed can be written as (6).

$$\omega_g = \omega_{m3} = -\omega_{m2} \quad (6)$$

After the one-way clutches, the torque T_s will be transferred to the output shaft and drives the generator as shown in (7), and the T_s equals to zero when absolute value of the input shaft speed ω_{m1} is slower than the output shaft speed ω_g.

$$(J_{s2} + J_{gb} + J_{cp2} + J_g)\dot{\omega}_g + (c_g + c_{vgb})\omega_g = T_s - T_e \quad (7)$$

where J_{s2} is the inertia of the output shaft; J_{gb} is the inertia of the bevel gearbox; J_{cp2} is the inertia of the lower mechanical coupling; J_g is the inertia of the generator; c_g is the viscous damping of the generator; c_{vgb} is the viscous damping of the gearbox;

T_e is the electrical torque derived from output load current of the generator as in (8) where p is the pole numbers, k_t is the torque constant of the generator, and i_{abc} are the current on each phase of the generator output. Phase to neutral air gap voltages E_{abc} (9) are the results of the rotor speed ω_g which is equals to the rotational speed of the output shaft in PTO, and the angle θ is decided by electric frequency $\omega_e = 0.5p\omega_g$. The air gap voltages can also be written as a function of current and internal impedances L_i and R_i in (10). The output resistive loads R_{in} is connected to the output of the generator.

$$T_e = \frac{p}{2} k_t [i_a \sin\theta + i_b \sin(\theta - \frac{2}{3}\pi) + i_c \sin(\theta + \frac{2}{3}\pi)] \quad (8)$$

$$\begin{cases} E_a = \sqrt{\frac{2}{3}} k_e \omega_g \sin\theta \\ E_b = \sqrt{\frac{2}{3}} k_e \omega_g \sin(\theta - \frac{2}{3}\pi) \\ E_c = \sqrt{\frac{2}{3}} k_e \omega_g \sin(\theta + \frac{2}{3}\pi) \end{cases} \quad (9)$$

$$\begin{cases} E_a = L_i(di_a/dt) + i_a(R_i + R_{in}) \\ E_b = L_i(di_b/dt) + i_b(R_i + R_{in}) \\ E_c = L_i(di_c/dt) + i_c(R_i + R_{in}) \end{cases} \quad (10)$$

As a result, the PTO system dynamic can be solved by including all the equations above including the nonlinear equations in (5).

III. Equivalent Circuit of Mechanical Motion Rectifier

The expression of dynamic equations is complicated and is difficult to analyse the frequency response of each component under different excitation input. The equivalent circuit model provides simple and straightforward understanding for the dynamics of the PTO under both time and frequency domain. Especially the nonlinear equations can be easily descripted by the electrical components in this section.

Fig. 3 shows the mechanism of the sprag one-way clutch and its equivalent circuit based on the analogue from (5) to the electrical equation (11) which shows the dynamics of the lower clutch, where the spring torsional coefficient is represented by the reciprocal of $L_{c3} = 1/k_{c3}$, and torsional damping coefficient is $R_{c3} = 1/c_{c3}$.

$$T_s = \begin{cases} (\omega_{m1} - \omega_{m3})/R_{c3} + \int(\omega_{m1} - \omega_{m3})dt\,/L_{c3} & if\ \omega_{m1} > \omega_{m3} \\ 0 & if \omega_{m1} < \omega_{m3} \end{cases} \quad (11)$$

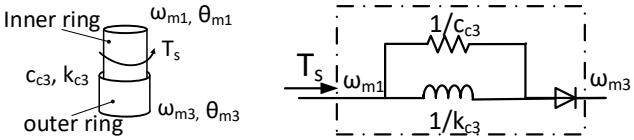

Fig. 3. The mechanical scheme and the equivalent circuit of the one-way sprag clutch. ω_{m1} θ_{m1} are the rotational speed and angle of the inner ring; ω_{m3} θ_{m3} are the rotational speed and angle of the outer ring; c_{sc3}, and k_{sc3} are the torsional damping and the torsional spring coefficient of the sprag clutch.

The nonlinear mechanism of the one-way clutch is represented by an ideal diode connected to a RL parallel network. The diode will only conduct when it anode voltage (p) is higher than the its cathode voltage (n). It can be analogue to (5) when ω_{m1} is smaller than ω_{m3} (ω_g), no torque is transmitted to the outer ring, whereas in this case no current will flow through the diode.

The rest of the model approximation can be derived based on the mechanical – electrical analogues introduced in [11] and Table I.

TABLE I
ANALOGUES BETWEEN MECHANICAL AND ELECTRICAL VARIABLES [11]

Mechanical	*Electrical*
Acceleration ($\ddot{x}$)	Current (i)
Velocity ($\dot{x}$)	Voltage (v)
Spring k: $dF/dt=k(\dot{x}_1-\dot{x}_2)$	Inductor 1/L: $di/dt=1/L(v_1-v_2)$
Inerter m: $F=m[d(\dot{x}_1-\dot{x}_2)/dt]$	Capacitor C: $i=C[d(v_1-v_2)/dt]$
Damper c: $F=c(\dot{x}_1-\dot{x}_2)$	Resistor 1/R: $i= (v_2-v_1)/R$

As a result, the PTO equivalent circuit model can be derived as following Fig. 4 where the ball-screw is represented as a

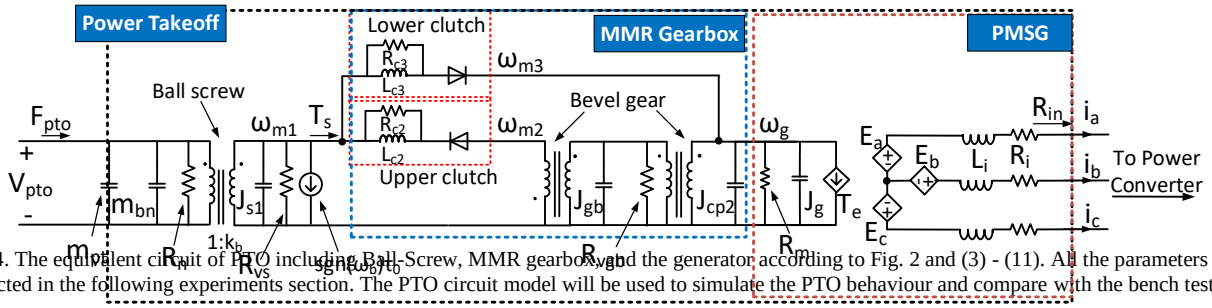

Fig. 4. The equivalent circuit of PTO including Ball-Screw, MMR gearbox and the generator according to Fig. 2 and (3) - (11). All the parameters will be extracted in the following experiments section. The PTO circuit model will be used to simulate the PTO behaviour and compare with the bench test results.

transformer with 1:k_b turn ratio; the mass and inertia are analogue to parallel capacitors along the circuit; the viscous dampers are analogue to the parallel resistors; the Coulomb friction τ_0 is analogue to a controlled current source based on the rotational direction; the 3-way bevel gears are analogue to the transformers with 1:1 ratio; two one-way clutches are analogue to the circuit in Fig. 3 with a RL network and ideal diode in series connection.

IV. Experimental Results and Analysis

Dry lab tests are performed with Instron machine 8801 to validate the equivalent circuit model in Fig. 4. A 500 W direct-drive PTO is used as a show case for the model, and its push tube is replaced to fit into the test machine. The test setup is shown in Fig. 5 that the PTO is fixed by clamps to prevent the rotational motion while driven linearly. The output setup of the PTO is shown in Fig. 5(b) that the three-phase generator is connected to three external resistors in Y configuration. The input force, displacement, and velocity are recorded by the data acquisition system on the test machine under 10 kHz of sampling frequency. The output information including two phase-neutral voltages, and two currents are recorded with oscilloscope under 20 kHz of sampling frequency.

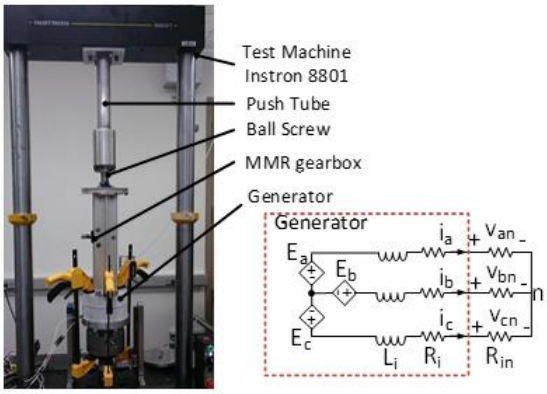

(a) (b)

Fig. 5. (a) PTO test setup with Instron 8801. The test machine will provide a linear actuation with triangular displacement or sinusoidal displacement to the tested PTO. (b) The PTO output setup of the three-phase generator, L_i and R_i are the internal inductors and resistors. R_{in} are the external resistances connected to the output of the generator.

To verify the equivalent viscous friction and the Coulomb friction, a triangular linear displacement is set as an input to the PTO where the input velocity can be assumed as a constant voltage source under steady state as in Fig. 6. The output voltage is almost constant during the test due to the square wave input from the test machine, and the input force is also a square wave under the test. The square force amplitude ΔF (12) is the result of the Coulomb friction and different viscous frictions under various input speed by assuming the diodes always conduct which can be simplified as Fig. 7(a). The capacitors and the inductors can assume to be open and short circuit under dc voltage input in Fig 4. The equivalent viscous friction c_e is derived in (13) as a sum of all the viscous frictions.

$$\Delta F_i = 2(k_b\tau_0 + v_{mi}{k_b}^2 c_e) \tag{12}$$

$$c_e = 1/R_e = c_n + {k_b}^2(c_{vs} + c_{vgb} + c_g) \tag{13}$$

where the ΔF_i is the different force amplitude according to different input velocity v_{mi}.

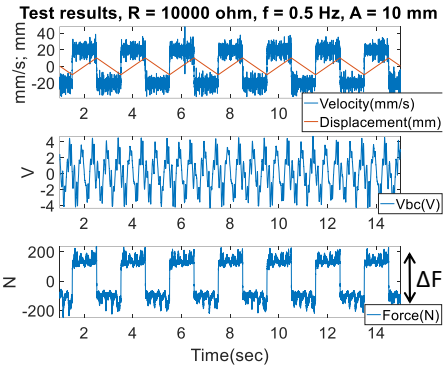

Fig. 6. The triangular displacement open circuit test for identification of PTO's characteristics. The velocity V_{mi}, displacement d_i, output voltage v_{bc}, and input force F_{pto} of PTO under 10 mm of amplitude, with square wave shape of velocity input.

The coefficient of the model (12) can be derived from the linear regression by using ΔF as a response and input velocity as an input control variable which can be shown in Fig. 7(b) that $2k_b\tau_0$ equals to 221.4 N, and ${k_b}^2c_e$ equals to 1305 Ns/m when k_b ratio is 104.

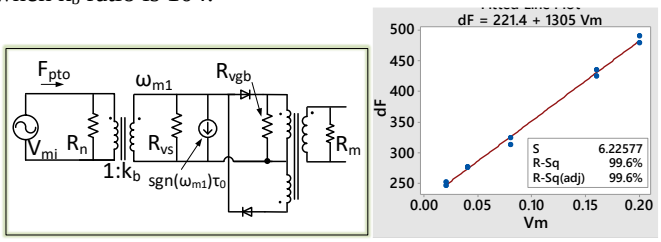

(a) (b)

Fig. 7. (a) Simplified equivalent circuit under constant velocity test (b) The ΔF – v_m curve with PTO input velocity v_m from under 0.02 – 0.2 m/s. According the linear regression results from Minitab, the equivalent coulomb friction is $2k_b\tau_0$=221.4 N, and the equivalent viscous friction is $2{k_b}^2c_e$ = 1305 Ns/m. In the simplified equivalent circuit, current source τ_0 = 1.06 A, and overall equivalent resistance $R_e = 1/c_e = R_n{k_b}^2//R_{vs}//R_{vgb}//R_m$ = 16.58 Ω.

The next step is to derive the L_{c2}, and L_{c3} in the equivalent circuit. This can be done by matching the efficiency curve of the PTO system. The mechanical efficiency of PTO is derived by measurement data from the input force and displacement, and the output voltage and currents as shown in the following equations (14) – (16)

$$P_{oe} = (I_aV_{an} + I_bV_{bn} + I_cV_{cn}) \tag{14}$$

$$P_{oe} = \frac{P_{oe}}{R_{in}}(R_{in} + R_i) \tag{15}$$

$$\eta_m = \frac{P_{om}}{P_{in}} \tag{16}$$

where the input power P_{in} is derived from the integral of the force and the displacement divided by the its time interval as in

Fig. 8; the output power P_o is derived from the mean value of the measured output voltage and current as shown in Fig. 5(b) and Fig. 8; η_m is the mechanical efficiency of the PTO; R_{in} is the external resistors connected as output loads for the generator; R_i is the internal resistance of the generator; here the voltage drop on the inductance L_i is neglected due to the relatively low impedance compared to R_i.

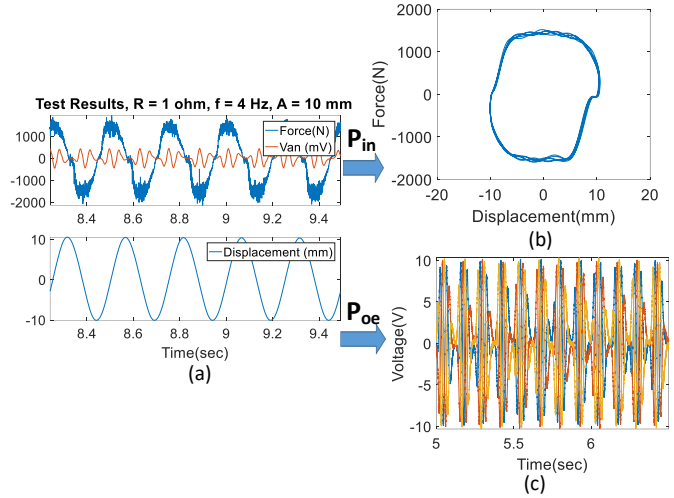

Fig. 8. (a) Bench test results under sinusoidal input displacement, amplitude as 10 mm of amplitude, 4 Hz of frequency, and 1 ohm of output resistance R_{in} (b) filtered force - displacement loop can be used to calculate the input power (c) measured three-phase output line-neutral voltage can be used to calculate the output power.

By assuming R_{c2} and R_{c3} equal to 50 ohm, values of L_{C2} and L_{c3} can be approximated as 0.07 H when compares the efficiencies from the bench test and the simulation results with different L_c values.

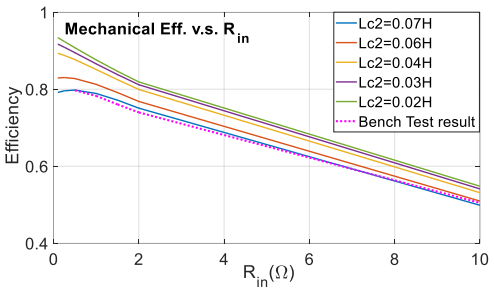

Fig. 9. Mechanical Efficiency to determine the inductance value L_c of both L_{c2} and L_{c3} under different output resistances from 0.1 Ω to 10 Ω. The simulated efficiency curve is approximated to the test results when L_c = 0.07 H.

Therefore, from the triangular input test results and the efficiency curve fitting under sinusoidal input test, all the parameters in the PTO equivalent circuit can be extracted. The developed model is then validated under real-time testing with multiple conditions as shown in Fig. 10 and Fig. 11. Under both test conditions the input force and the output voltage can fit between the experiment and simulation results, besides the noise from the measured input force might be the result from gears engagements and other non-ideal effects from the mechanical coupling.

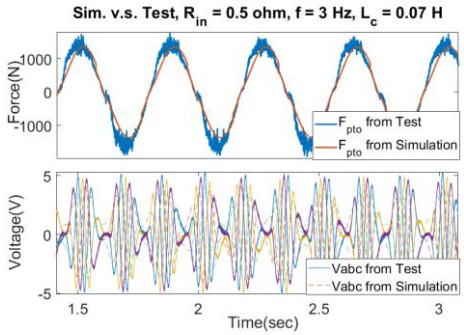

Fig. 10. Time domain results of PTO input force F_{pto} and output voltage Vabc from the Fig. 5 bench test and Fig. 4 simulation under R_{in} = 0.5 Ω, 3 Hz of driving frequency, and 10 mm of amplitude.

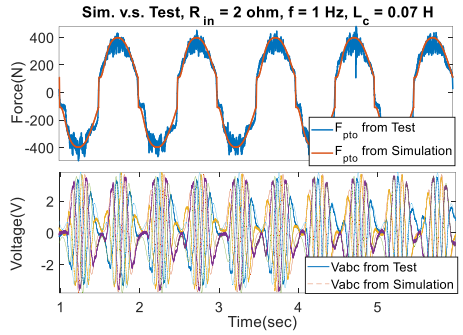

Fig. 11. Time domain results of PTO input force F_{pto} and output voltage Vabc from the Fig. 5 bench test and Fig. 4 simulation under R_{in} = 0.5 Ω, 3 Hz of driving frequency, and 10 mm of amplitude.

V. Conclusions

An equivalent circuit for MMR-based PTO is derived. The MMR gearbox can be shown as a parallel RL network series connected to an ideal diode. The parameter extractions are extracted through bench tests. Finally, the derived model can accurately predict the PTO input force and its efficiency, and it can further combine with a circuit-based W2W model for overall WEC system simulation.

Acknowledgment

This work was supported by the MHK Program of Department of Energy under Award Number EE0007174, and the National Science Foundation (NSF 1530122).

References

[1] Y. K. Ramadass and A. P. Chandrakasan, "An efficient piezoelectric energy harvesting interface circuit using a bias-flip rectifier and shared inductor," *IEEE J. Solid-State Circuits*, vol. 45, no. 1, pp. 189–204, 2010.

[2] M. Villalva, J. Gazoli, and E. Filho, "Comprehensive Approach to Modeling and Simulation of Photovoltaic Arrays," *IEEE Trans. Power Electron.*, vol. 24, no. 5, pp. 1198–1208, 2009.

[3] S. Cao, S. Yang, J. Zheng, L. Zhang, and B. Wang, "An Equivalent Circuit Model and Energy Extraction Technique of a Magnetostrictive Energy Harvester," *IEEE Trans. Appl. Supercond.*, vol. 26, no. 4, 2016.

[4] J. Falnes, *Ocean waves and oscillating systems : linear interactions including wave-energy extraction*. Cambridge University Press, 2002.

[5] X. Li *et al.*, "Design , fabrication and testing of wave energy converters using different power take-off with mechanical motion rectifier," pp. 1–7, 2017.

[6] Z. Li, L. Zuo, J. Kuang, and G. Luhrs, “Energy-harvesting shock absorber with a mechanical motion rectifier,” *Smart Mater. Struct.*, vol. 22, no. 2, p. 25008, 2013.
[7] “http://www.wcbranham.com/gearboxes-right-angle/branham-spiral-bevels/4304-0416/.” .
[8] L. Koyo Seiko CO., “Sprag Type One-Way Clutches: For Automobiles.”
[9] P. Ricci, J. -B. Saulnier, A. F. de O. Falcão, and M. T. Pontes, “Time-Domain Models and Wave Energy Converters Performance Assessment,” *Vol. 6 Nick Newman Symp. Mar. Hydrodyn. Yoshida Maeda Spec. Symp. Ocean Sp. Util. Spec. Symp. Offshore Renew. Energy*, vol. 6, no. March 2016, pp. 699–708, 2008.
[10] J. V. Ringwood, G. Bacelli, and F. Fusco, “Energy-maximizing control of wave-energy converters: The development of control system technology to optimize their operation,” *IEEE Control Syst.*, vol. 34, no. 5, pp. 30–55, 2014.
[11] M. C. Smith, “Synthesis of mechanical networks: The inerter,” *IEEE Trans. Automat. Contr.*, vol. 47, no. 10, pp. 1648–1662, 2002.